Quasi-free-space optical coupling between diffraction grating couplers fabricated on independent substrates

Anthony V. Mulé, Ricardo Villalaz, Thomas K. Gaylord, and James D. Meindl

Optical coupling between preferential-order volume diffraction grating couplers fabricated on independent substrates is demonstrated. The coupling efficiency between gratings is quantified as a function of both grating and waveguide fabrication technology and relative angular position of the two substrates. A maximum grating-to-grating coupling efficiency of 31% is reported for coupling between two nonoptimized, nonfocusing, unpatterned volume grating couplers. © 2004 Optical Society of America

OCIS codes: 050.7330, 130.2790, 200.4650, 230.7380.

1. Introduction

The successful merging of optical interconnect and silicon complementary metal-oxide semiconductor technologies for chip-to-chip communication is challenged by the need for efficient optical coupling between sources and detectors located on independent substrates. Free-space coupling between separate substrates addresses the challenge of optical coupling involving off-chip light sources at the cost of increased system volume and associated packaging costs. In contrast, guided-wave optical interconnect systems offer compact packaging and fabrication technologies that are compatible with printed wiring board manufacture.[1] The success of guided-wave interconnect systems, however, is challenged by the need for optical coupling between waveguides located on separate two-dimensional planes of propagation (such as board-level and chip-level waveguides, for example). Surface-normal optical coupling between waveguides located on the *same* substrate has been demonstrated by use of vertical waveguide bends[2] and vertical directional couplers,[3–5] for example. The use of vertical waveguide bends implies the location of source and detector on the same substrate. The extension of vertical directional coupling to optical coupling between waveguides located on separate substrates would require coupling lengths of the order of or greater than silicon complementary metal-oxide semiconductor chip dimensions, as board and chip substrates are separated by distances of the order of solder ball dimensions (i.e., tens of micrometers),[6] and the large refractive-index contrast Δn between waveguide core and intermediate dielectric regions would result in coupling lengths of the order of or greater than several millimeters, depending on the value of Δn.[7]

The use of diffractive grating couplers for surface-normal coupling between optical waveguides has also been investigated. Numerical simulations for a nonpreferential-grating-assisted waveguide-to-waveguide coupler that uses nonterminated waveguides and photonic bandgap structures predict coupling efficiencies between waveguides of 33.6% and 17.6% for the forward- and backward-propagating modes, respectively,[8] excited within the receiving waveguide. Wavelength-selective, contradirectional, radiation-mode coupling between nonpreferential surface-relief gratings has also been reported.[9,10] Values for measured coupling efficiency involving stacks of two[9] and three[10] gratings are reported as a few percent and as 5%, respectively. All these approaches, however, involve coupling between gratings stacked vertically on the same substrate. In addition, the use of nonpreferential surface-relief gratings implies the loss of power diffracted into the substrate or cover regions for gratings designed to diffract into the cover or substrate regions. The use of preferential-order volume diffraction gratings for grating-to-grating coupling max-

The authors are with the Microelectronics Research Center, Georgia Institute of Technology, Atlanta, Georgia 30332-0269. A. V. Mulé's e-mail address is gt2925a@prism.gatech.edu.

Received 25 February 2004; revised manuscript received 29 June 2004; accepted 12 July 2004.

0003-6935/04/295468-08$15.00/0

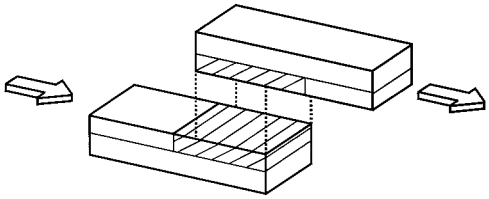

Fig. 1. Grating-to-grating coupling.

imizes the power diffracted into the target diffracted order and allows for a simplification of the grating fabrication sequence compared with that of preferential-order surface-relief gratings. In addition, the interferometric process used to define volume diffraction gratings can provide higher-fidelity grating profiles than the wet- or dry-etch chemistry–based processes used to produce surface-relief gratings.[11]

This research demonstrates, for the first time to our knowledge, optical coupling between preferential-order, volume diffraction grating couplers located on independent substrates (Fig. 1). Both slab, planar grating couplers and grating couplers patterned into isolated channels are coupled optically to characterize the effect of grating fabrication technology on grating-to-grating coupling efficiency. The fabrication of diffraction gratings on separate substrates allows for a preliminary investigation into the angular tolerances associated with grating-to-grating coupling efficiency with respect to relative substrate position.

2. Fabrication and Characterization of Grating Coupler Substrates

Measurements of coupling efficiency between gratings located on separate substrates involve the optical excitation of a base grating substrate fixed to a translation stage and excited by an optical fiber. The base substrate consists of either finite-width channel gratings or a slab (~10-mm-wide) grating. Light diffracted by the substrate volume grating is coupled into a second volume grating that resides on a transparent substrate that is suspended over the first. Both unpatterned, slab gratings and patterned, channel waveguide gratings were fabricated from Omnidex HRF-600 laminate photopolymer from DuPont. The fabrication of both unpatterned and patterned gratings begins with the interferometric recording of grating fringes within a 6-μm-thick Omnidex film laminated atop a fused-silica substrate.[11] Slab, nonfocusing, preferential-order volume grating couplers with period $\Lambda = 0.3$ μm and slant angle $\Phi = 45°$ are created by use of a two-beam interferometric exposure. The grating profile, defined through monomer–polymer diffusion, is locked before film cure with an additional uniform one-beam exposure. Each substrate is placed atop a hot plate heated to the curing temperature of the film (120–150 °C) for a short period before the remaining Mylar film that originally encased the laminate Omnidex film is removed.

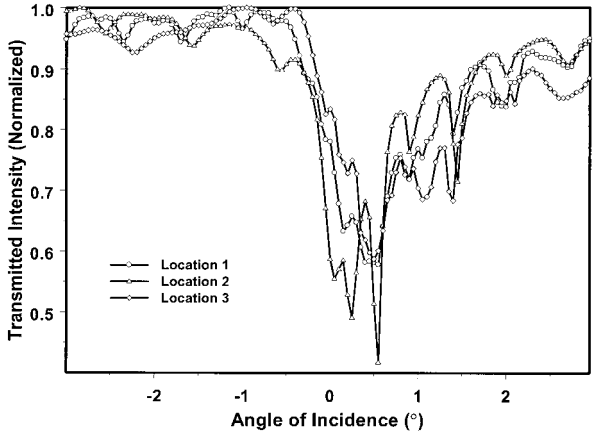

Fig. 2. Angular selectivity measurements of the top substrate grating before channel patterning. A peak input coupling efficiency of 59% is visible. Each minimum corresponds to Bragg coupling of the incident test beam to a waveguide mode supported by the grating film.

After removal of the Mylar, each sample is cured and tested with respect to input coupling efficiency and Bragg angle before patterning. Figure 2 depicts input coupling efficiency measurements as a function of location for the grating corresponding to the top slab grating substrate during grating-to-grating coupling measurements. We obtained the data of Fig. 2 by mounting the grating sample atop a rotation stage and observing the transmitted intensity of a collimated TE-polarized He–Ne test beam as a function of rotation angle, thereby producing the angular selectivity profile of a volume diffraction grating. Each measurement location refers to a unique position of the test beam along the waveguide–grating interface, where the waveguide region within slab grating samples is represented by unexposed Omnidex photopolymer. All volume gratings fabricated for this study were fabricated as grating-in-the-waveguide volume diffraction gratings[12] as opposed to grating-on-the-waveguide volume diffraction gratings.[11] For grating-in-the-waveguide volume gratings, the lines of refractive-index modulation that represent the grating profile are written within the volume of the grating photopolymer material, which supports several vertical optical modes. Each dip in transmitted intensity within the angular selectivity profile corresponds to optical diffraction of incident light into a mode supported by the Omnidex film, where each mode is associated with a unique Bragg angle of diffraction.

After angular characterization, a portion of the slab grating test substrates is transformed into patterned grating channels. Each patterned grating test substrate consists of ten to twelve 100-μm-wide grating channels defined with a center-to-center spacing of 650 μm by use of a metal hard mask and by O_2-based reactive-ion etch processing. Following reactive-ion etch definition of grating channel regions, each sample is etched briefly in a buffered oxide etch solution to undercut and remove Omnidex

film residue to complete the channel patterning process. The choice of 100/650-μm width/pitch channels balances the desire for isolated waveguide channels with the requirement of grating channel performance dominated by optical diffraction rather than by channel sidewall scattering. The fabrication technology employed to produce patterned substrates, however, could be applied to produce narrower grating channels for increased interconnect density in future studies.

Omnidex HRF photopolymer is optimized for holographic grating recording[13–16] and is not intended for use as an optical waveguide material. As such, Omnidex films exhibit intrinsic absorption losses of ~5 dB/cm (Ref. 17) and prohibitive sidewall scattering along reactive-ion etch–patterned waveguide channels. To implement low-loss waveguides, Avatrel 2190P negative-tone photopolymer from Promerus llc, is used, in which raised-strip channels are photodefined atop and lead into patterned grating channel regions. We promote adhesion between Avatrel and Omnidex films by depositing 0.12 μm of SiO_2 atop the patterned grating substrates, using plasma-enhanced chemical-vapor deposition before the Avatrel photopolymer is deposited and processed. The deposition temperature of the SiO_2 film is kept at or below the cure temperature of the Omnidex film to prevent degradation of grating coupler performance at temperatures typically associated with SiO_2 plasma-enhanced chemical-vapor deposition (i.e., ≥300 °C). Each waveguide channel is 125 μm wide, resulting in the presence of Avatrel photopolymer on either side of Omnidex gratings to passivate the rough plasma-defined Omnidex sidewalls. Although the use of waveguides with widths greater than that of the grating channels causes to a portion of the guided light to bypass the grating channels, the large width of the grating channels ensures that sufficient light interacts with and is coupled by diffraction grating regions. The butt coupling of Avatrel waveguide channels into Omnidex gratings channels can provide scatter-free Avatrel–Omnidex interfaces with proper processing because of the small value of Δn between Avatrel ($n = 1.5161$) and Omnidex ($n = 1.5103$) at the optical test wavelength $\lambda = 632$ nm (i.e., $\Delta n = 5.8 \times 10^{-3}$).[18]

When Avatrel is spin coated atop a planar slab grating, the Avatrel encapsulation layer smooths the surface profile of the air–polymer interface and enhances the peak input coupling efficiency. Figure 3 illustrates rotation stage measurements of a slab volume grating coupler both before and after encapsulation. An increase of 14% in the magnitude of the minimum corresponding to the Bragg angle of the fundamental mode with encapsulation can be observed. The application of Avatrel to the nonplanar grating channel topology, however, results in the formation of raised polymer features atop each grating channel. Figure 4 illustrates optical profilometer scan data of Avatrel-encapsulated, patterned Omnidex grating channels. The nonplanar topology of the Avatrel polymer region above the diffraction grating coupler is clearly visible. To investigate the effect of Avatrel encapsulation on grating-to-grating coupling efficiency, we therefore encapsulate a portion of unpatterned, slab grating test substrates (and all test substrates with patterned grating channels) in Avatrel.

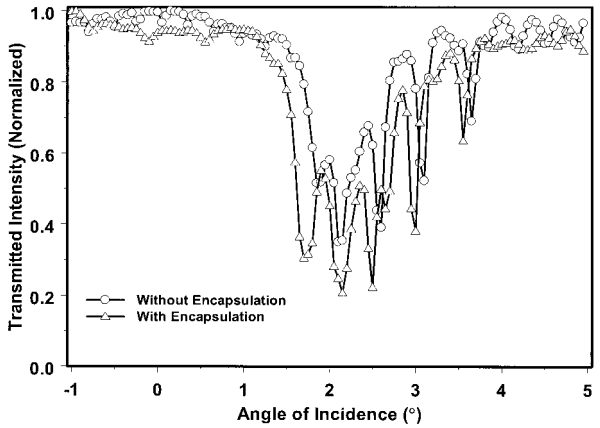

Fig. 3. Angular selectivity measurements of slab Omnidex grating both before and after encapsulation in Avatrel. An increase of 14% in the peak input coupling efficiency is visible following encapsulation.

A micrograph of the top substrate following grating channel patterning is depicted in Fig. 5. Angular selectivity measurements of the grating couplers depicted in Fig. 5 are shown in Fig. 6; each measure-

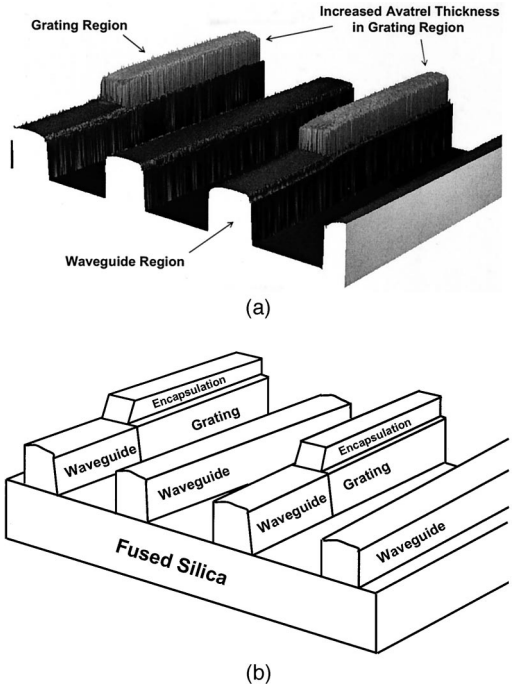

Fig. 4. (a) Optical profilometer scan of Avatrel-encapsulated volume grating channels. The nature of Avatrel is such that a nonplanar topology results when the material is spun atop a nonplanar substrate. The thickness of the interconnect increases in the grating region by the thickness of the applied Avatrel film. (b) Diagram of optical profilometer scan data.

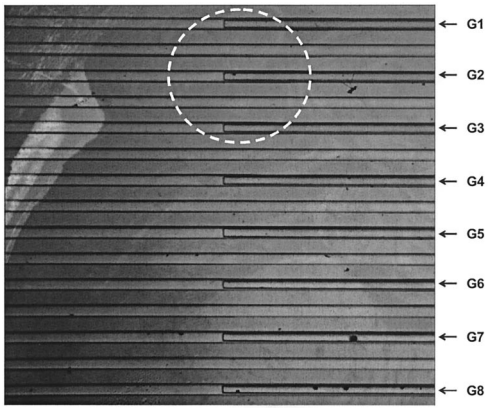

Fig. 5. Top-view micrograph of a substrate with grating-in-the-waveguide optical interconnect channels G1–G8. Dashed circle, area encompassed by the He–Ne test beam for location 1 depicted in Fig. 6.

ment location referenced in Fig. 6 refers to a unique placement of the He–Ne test beam along the waveguide–grating interface of multiple channels. As the substrate under test has patterned channels, the majority of light corresponding to the approximately 800-μm-(FWHM) diameter He–Ne test beam passes through nongrating regions. Hence, the magnitudes of the dips in transmitted intensity in Fig. 6 are reduced compared with those of Fig. 2. The Bragg angle of coupling for the fundamental and other modes of the Omnidex film, however, are in agreement with those depicted in Fig. 2, indicating that the processing associated with the formation of air-clad, two-material, grating-in-the-waveguide volume grating waveguide channels does not affect the basic functionality of the gratings.

Optical characterization of patterned top and bottom substrates is made with respect to the propagation loss of the waveguide leading into each grating region (α_{wg}) and to the coupling coefficient of each diffraction grating (α_g). We evaluate α_{wg} and α_g by

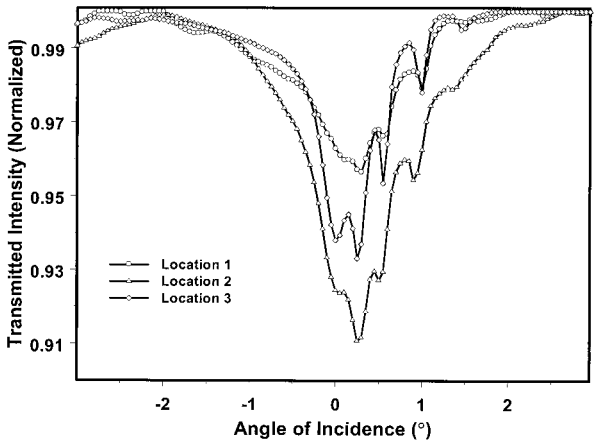

Fig. 6. Angular selectivity measurements of the top substrate grating following channel patterning. The magnitude of the minimum is reduced because of the small (3%) overlap between the He–Ne test beam and the patterned grating channels.

Table 1. Summary of Grating Coupling Coefficients and Lengths for Bottom and Top Test Substrates[a]

	Bottom Substrate		Top Substrate	
Grating Channel	Coupling Coefficient (mm^{-1})	Grating Length (μm)[b]	Coupling Coefficient (mm^{-1})	Grating Length (μm)[b]
G1	4.63	234	NA	NA
G2	1.71	446	5.30	438
G3	3.07	246	1.56	220
G4	1.77	441	3.14	289
G5	NA	NA	1.93	382
G6	1.72	226	NA	NA
G8	3.38	264	NA	NA

[a]NA, not available.
[b]Length of region over which data were fitted.

capturing an image of the scattered and the diffracted intensity patterns, respectively, and loading the image into an analytical software package such as Matlab. The intensity profiles are then fitted to an exponential by use of robust bisquare linear least-squares fit algorithm.[19] Tables 1 and 2 provide summaries of α_g and α_{wg}, respectively, for patterned substrates used in this study. Coupling coefficient α_g ranges from 1.56 to 5.3 mm^{-1}; propagation loss coefficient α_{wg} ranges from −0.47 to −10.5dB/cm for the channels listed in Tables 1 and 2. More information regarding the fabrication and performance of the grating channels listed in Tables 1 and 2 is reported elsewhere.[18]

3. Grating-to-Grating Coupling Efficiency

We measure the grating-to-grating coupling efficiency by monitoring the optical power diffracted from the bottom substrate grating as it is transmitted through the top substrate grating. The top substrate grating is suspended above the first in a manner such that the relative planar and angular positions of the top substrate are controlled with high fidelity. The measurement configuration used to quantify the grating-to-grating coupling efficiency is illustrated in Fig. 7. Control of the three planar degrees of freedom is achieved with an x–y–z translation stage, where x, y, and z are defined as the

Table 2. Summary of Propagation Loss Metrics for Avatrel Waveguide Segments Leading to Diffraction Gratings Located on the Bottom and Top Test Substrates[a]

	Bottom Substrate		Top Substrate	
Grating Channel	Loss (dB/cm)	Length (μm)[b]	Loss (dB/cm)	Length (μm)[b]
G2	−10.5	1955	−0.47	2827
G3	−1.49	1059	−0.76	2601
G4	−6.89	4250	NA	NA
G5	NA	NA	−3.09	2807
G8	−7.08	1755	NA	NA

[a]NA, not available.
[b]Length of region over which data were fitted.

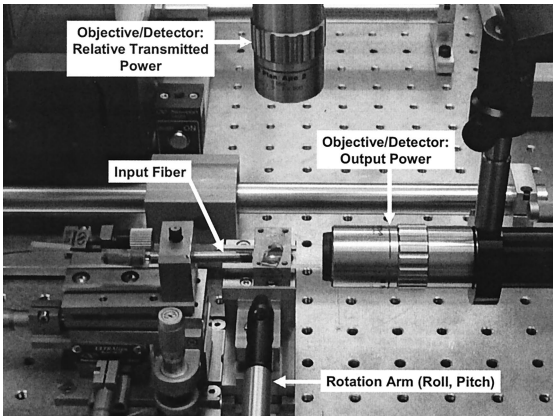

Fig. 7. Grating-to-grating coupling efficiency measurement configuration. The top substrate is suspended above the bottom substrate during measurement by the rotation arm such that the relative lateral, longitudinal, and vertical positions of the top substrate are controlled with micrometer resolution. The relative roll and pitch of the top substrate are controlled to within 0.02°, whereas the relative yaw is minimized by alignment of waveguides on both substrates through visual inspection with the translatable microscope.

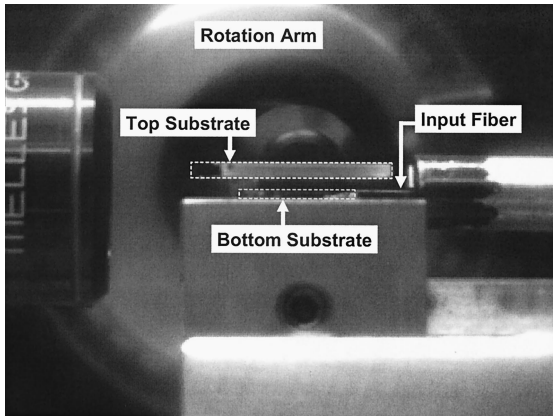

Fig. 8. Image of top and bottom substrates taken during pitch initialization. The relative angular position of the top substrate is initialized to ~0°.

longitudinal, lateral, and vertical directions, respectively. The longitudinal direction is defined as the direction of the propagation of light within the waveguide channels; the vertical direction is that between gratings. In addition, roll, pitch, and yaw are defined as angular rotations about the x, y, and z axes, respectively. To control the relative roll and pitch of the top and bottom substrates, we couple two rotation stages and attach them to the translation stage. An extension arm terminated with a flexible plastic clamp is attached to the rotation stage controlling pitch and is used to hold the top substrate in place during measurements. Control over the relative yaw of the two substrates is achieved through visual inspection.

Initialization of the six degrees of freedom of the top substrate relative to the bottom substrate is required before the start of measurements. We set the longitudinal and lateral positions of the top substrate periodically during measurements by adjusting the x–y–z stage longitudinal and lateral micrometers. Before determining the relative vertical position of the top substrate, we must first set the roll and pitch to 0°. To initialize the pitch we mount a CCD camera with a 5× microscope objective looking laterally into the rotation arm, as shown in Fig. 8. After images of the two substrates are captured, the image is loaded into a photoeditor software package and the relative angle between the two substrates is approximated. After the relative pitch between the two substrates is determined, the top substrate is rotated accordingly, and the process is repeated until the top substrate lies at a relative pitch of approximately 0°. An absolute relative pitch of 0° is not essential because (a) the goal of the measurement is to observe the tolerance of grating-to-grating coupling with respect to pitch angle (thereby placing more importance on knowledge of the pitch increment applied during a measurement) and (b) the Bragg angles of the gratings are already known. An approximation of 0° is important for determining a minimum safe vertical height at which the top substrate must reside for a given pitch angle to prevent the top substrate from making contact with the bottom substrate or input fiber. After the relative pitch of the top substrate is initialized, the roll is initialized in a similar fashion. Once the pitch and the roll are set to 0° we find the relative vertical height of the top substrate by comparing the vertical micrometer settings of the end-view camera when the output facet of a waveguide on either substrate is brought into focus relative to a common reference point on a TV monitor.

With the angular degrees of freedom initialized and the relevant controlling stages calibrated, the bottom substrate is excited with the input fiber, and an investigation of the grating-to-grating coupling efficiency can be conducted. Two methods for quantifying grating-to-grating coupling efficiency were investigated. The first method is based on measuring the power coupled into the top substrate waveguide–grating channel by observing the output of the waveguide and comparing the measured output power with that diffracted by the bottom substrate waveguide–grating channel. The success of this end-view method is challenged by the need to introduce an aperture between the waveguide output and the detector in order to discard unwanted background light stemming from sources outside the top–substrate waveguide, including light associated with the output of the bottom substrate waveguide excited by the optical fiber. In addition to the need for an aperture on the detector, monitoring of optical power emitted from the top substrate waveguide implies a translation of the end-view camera–detector pair with each angular, longitudinal, lateral, or vertical increment or combination of any of these. The measurement of grating-to-grating-coupled power in this manner, therefore, can require excessive time and effort. Although significant challenges are associ-

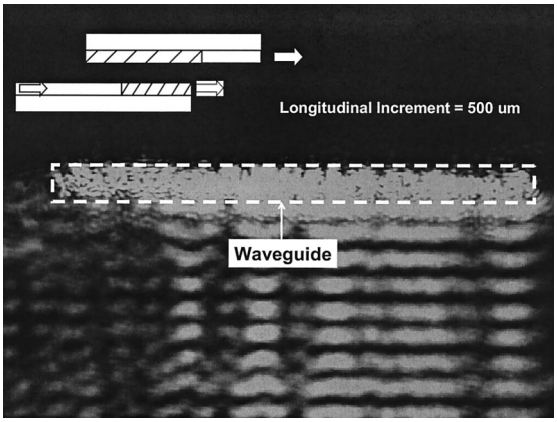

Fig. 9. Grating-to-grating coupling when the patterned top substrate is incremented longitudinally to couple optically to the bottom patterned substrate. The vertical separation between substrates is 500 μm.

ated with the end-view method with respect to accurate optical power measurements, one can gain insight into the dependence of grating-to-grating coupling efficiency on the relative position of the top substrate by monitoring the top substrate waveguide–grating output under various relative positions. For example, Fig. 9 depicts the top substrate waveguide output when the relative longitudinal position of the waveguide–grating interface of each substrate is optimized. In addition, the dependence of coupling efficiency on the relative height of the top substrate can be seen from Fig. 10, where grating-to-grating coupling is observed when the top substrate is placed at a vertical distance of 5 mm above the bottom substrate.

The second method of quantifying grating-to-grating coupling efficiency involves monitoring the power diffracted from the bottom substrate grating through the top substrate grating as a function of relative position. In this manner the need for aperturing unfocused background light during the measurement of power coupled between gratings is eliminated. In addition, the position of the camera–detector is kept constant throughout the translation

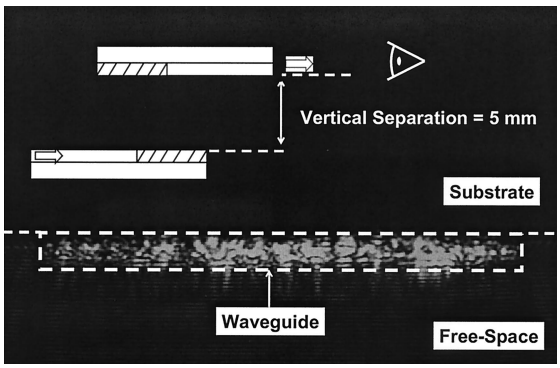

Fig. 10. Grating-to-grating coupling when the top substrate is 5 mm above the bottom substrate. Note the absence of unfocused background light beneath the waveguide.

of the top substrate, thereby simplifying the process and reducing measurement time. Finally, the relative nature of this measurement adds further simplification by eliminating the need to measure absolute power levels, which can be influenced by many factors such as off-axis camera position that can vary between measurements. This top-view method of quantifying grating-to-grating coupling efficiency essentially amounts to repeating the rotation stage measurements conducted with the He–Ne test beam, as both involve monitoring power transmitted through a grating substrate as a function of pitch angle of rotation. The only difference associated with the top-view method is the replacement of the He–Ne test beam with optical power diffracted by a second diffraction grating. The dips in transmitted intensity recorded with the top-view method during grating-to-grating coupling measurements, therefore, correspond to power diffracted into various modes of the top substrate grating film. As these dips are measured by use of grating-in-the-waveguide volume grating couplers, the measurement of power diffracted by the top substrate grating represents the measurement of vertical, quasi-free-space optical coupling between two grating-enabled waveguides located on independent substrates. Given the small value of Δn between Avatrel waveguide and Omnidex grating materials at the optical test wavelength, excitation of one of more of the vertical modes supported by the Avatrel waveguides (in the case of patterned substrates) also occurs, as shown in Figs. 9 and 10.

To monitor the transmitted power, a 20× infinity-corrected objective is attached to a 2× microscope tube mounted within a microscope stand. First a CCD camera is mounted on the microscope tube to bring the bottom substrate grating under test into view. Once the microscope objective and the tube are aligned properly, the top substrate is mounted into place, and the surface of the top substrate grating is brought into focus. At this point the CCD camera is replaced with a picowatt detector, and the diffracted power is ready to be monitored. Table 3 summarizes the peak input coupling efficiency measured for multiple test cases involving both unpatterned and patterned volume gratings.

The first two test cases of Table 3 involve grating-to-grating coupling between unpatterned diffraction grating couplers. The optical coupling of unpatterned grating substrates provides the most accurate insight into the basic nature of grating-to-grating coupling, as the effect of interconnect fabrication technology is minimized. Cases 1 and 2 of Table 3 correspond to the configurations in which a passivated and an unpassivated unpatterned top grating substrate, respectively, couple optically to an unpatterned, unpassivated bottom substrate. In both cases (depicted in Figs. 11 and 12, respectively), a clear, uniform dip in the transmitted intensity is produced as the top substrate is rotated about the bottom substrate toward the Bragg angle of the fundamental mode. Cases 3 and 4 involve the optical coupling

Table 3. Summary of Grating-to-Grating Coupling Efficiency Measurements

Case Number	Bottom Substrate		Top Substrate		Peak Grating-to-Grating Coupling Efficiency (%)
	Patterned?	Encapsulated?	Patterned?	Encapsulated?	
1	No	No	No	Yes	23.0–31.0
2	No	No	No	No	28.4
3	Yes	Yes	No	Yes	26.0
4	Yes	Yes	No	No	19.1–19.8
5	No	No	Yes	Yes	3.0
6	Yes	Yes	Yes	Yes	4.5–12.0

between a patterned bottom grating and an unpatterned top grating, and cases 5 and 6 include grating-to-grating coupling involving a patterned top grating. In contrast to those of cases 1 and 2, the measurement data of cases 3–6 include the effects of interconnect fabrication technology on grating-to-grating coupling. Specifically, the presence of patterned channels involving Avatrel-encapsulated gratings includes the effect of the nonplanar surface topology depicted in Fig. 3. Owing to the presence of these nonplanar features, the peak grating-to-grating coupling efficiencies should be less than those of the first two test cases. The peak grating-to-grating coupling efficiencies listed for cases 3–6 suggest that the effect of patterned grating channels is most pronounced for the configurations involving a patterned top substrate. A clear decrease in the coupling efficiency can be observed between cases 4 and 6 with the introduction of a patterned top substrate into the coupling path. The reduction in coupling efficiency between cases 3 and 4 can be attributed to the effect of the Avatrel encapsulation layer, as demonstrated in Fig. 3. The optical coupling between a patterned top substrate and an unpatterned bottom substrate (case 5) exhibits a significant reduction in peak grating-to-grating coupling efficiency that is due to the small (8.5%) overlap between the diffracted intensity profile of the bottom substrate grating and the patterned top substrate grating.

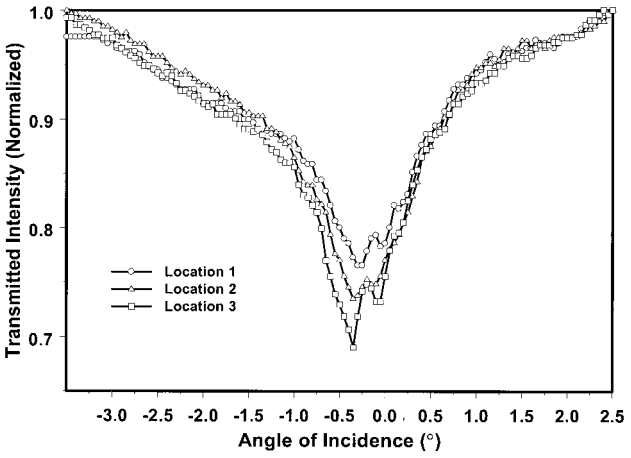

Fig. 11. Grating-to-grating angular selectivity measurement data corresponding to an unpatterned bottom substrate with an unencapsulated grating coupled optically to an unpatterned top substrate with an encapsulated grating (case 1 of Table 3). Each data set corresponds to a different test location on the top substrate. The peak grating-to-grating coupling efficiency is 31%.

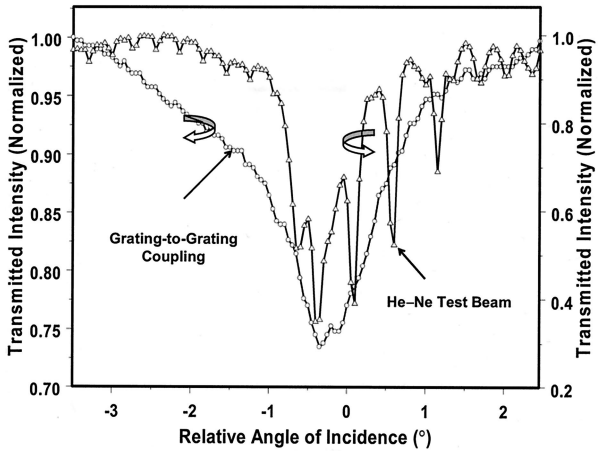

Fig. 12. Grating-to-grating angular selectivity measurement data corresponding to an unpatterned bottom substrate with an unencapsulated grating coupled optically to an unpatterned top substrate with an unencapsulated grating (case 2 of Table 3). The peak grating-to-grating coupling efficiency is 28.4%. The angular selectivity data of the top substrate when it is tested with the He–Ne test beam is also shown to demonstrate the increased angular tolerance with respect to pitch angle of incidence that results during grating-to-grating coupling.

An important observation highlighted in Fig. 12 is the smoothing of the angular selectivity profile of the grating under test when a second grating represents the optical excitation source. In contrast to the pronounced selectivity exhibited when the grating under test is excited by a collimated He–Ne test beam (right-hand axis of Fig. 12), the finite angular spread associated with the diffracted output of a volume grating satisfies the Bragg condition of each mode supported by the grating film in a more continuous manner (left-hand axis of Fig. 12). This increased continuity translates into higher tolerance with respect to the relative pitch angle of the top substrate.

4. Conclusions

Optical coupling between waveguide-embedded volume grating couplers located on independent substrates has been demonstrated for the first time to the authors' knowledge. Peak grating-to-grating coupling efficiencies as large as 31%, depending on

substrate fabrication technology, were observed. Coupling efficiency can be observed to be strongest between unpatterned substrates, whereas coupling between patterned, encapsulated substrates is lower because of the nonplanar topography of the encapsulating layer. The gratings designed, fabricated, and tested in the research reported here have a single period and thus are nonfocusing devices. The gratings are optimized neither for outcoupling nor for incoupling. It is anticipated that design optimization of the gratings will substantially improve the grating-to-grating coupling efficiency. Improved waveguide polymer materials that produce planar topologies when they are applied to nonplanar surfaces, the fabrication of patterned grating channels without Avatrel passivation, and the development of a polymer material suitable for both waveguide and grating applications represent possible solutions with which to address the reduced grating-to-grating coupling efficiency observed between substrates with patterned diffraction grating channels.

The authors thank Amy Fuertes for her help in collecting experimental data. This research is supported by the Semiconductor Research Corporation and the Microelectronics Advanced Research Corporation.

References

1. A. V. Mulé, E. N. Glytsis, T. K. Gaylord, and J. D. Meindl, "Electrical and optical clock distribution networks for gigascale microprocessors," IEEE Trans. Very Large Scale Integr. (VLSI) Syst. **10,** 582–594 (2002).
2. S. M. Garner, S.-S. Lee, V. Chuyanov, A. Chen, A. Yacoubian, W. H. Steier, and L. R. Dalton, "Three-dimensional integrated optics using polymers," IEEE J. Quantum Electron. **35,** 1146–1155 (1999).
3. P. C. Noutsios, G. L. Yip, and J. Albert, "Novel vertical directional coupler made by field-assisted ion-exchanged slab waveguides in glass," Electron. Lett. **28,** 1340–1342 (1992).
4. M. Raburn, B. Liu, P. Abraham, and J. E. Bowers, "Double-bonded InP-InGaAsP vertical coupler 1:8 beam splitter," IEEE Photon. Technol. Lett. **12,** 1639–1641 (2000).
5. S. June Choi, K. Djordjev, S. Jun Choi, P. D. Dapkus, W. Lin, G. Griffel, R. Menna, and J. Connolly, "Microring resonators vertically coupled to buried heterostructure bus waveguides," IEEE Photon. Technol. Lett. **16,** 828–830 (2004).
6. J. Link and V. Solberg, "Placement and reflow of 0.3mm diameter solder balls for chip-scale μBGA devices," Chip Scale Rev. **1,** 28–35 (1997).
7. J. Kobayashi, T. Matsuura, S. Sasaki, and T. Maruno, "Directional couplers using fluorinated polyimide waveguides," J. Lightwave Technol. **16,** 610–614 (1998).
8. T. Liang and R. W. Ziolkowski, "Grating assisted waveguide-to-waveguide couplers," IEEE Photon. Technol. Lett. **10,** 693–695 (1998).
9. Q. D. Xing, S. Ura, T. Suhara, and H. Nishihara, "Contradirectional coupling between stacked waveguides using grating couplers," Opt. Commun. **144,** 180–182 (1997).
10. S. Ura, R. Nishida, T. Suhara, and H. Nishihara, "Wavelength-selective coupling among three vertically integrated optical waveguides by grating couplers," IEEE Photon. Technol. Lett. **13,** 133–135 (2001).
11. S. M. Schultz, E. N. Glytsis, and T. K. Gaylord, "Volume grating preferential-order focusing waveguide coupler," Opt. Lett. **24,** 1708–1710 (1999).
12. M. L. Jones, R. P. Kenan, and C. M. Verber, "Rectangular characteristic gratings for waveguide input and output coupling," Appl. Opt. **34,** 4149–4158 (1995).
13. W. J. Gambogi, W. A. Gerstadt, S. R. Makara, and A. M. Weber, "Holographic transmission elements using improved photopolymer films," in *Computer and Optically Generated Holographic Optics*, I. Cindrich and S. H. Lee, eds., Proc. SPIE **1555,** 256–267 (1991).
14. W. J. Gambogi, A. M. Weber, and T. J. Trout, "Advances and applications of DuPont holographic photopolymers," in *Holographic Imaging and Materials*, T. H. Jeong, ed., Proc. SPIE **2043,** 2–13 (1994).
15. T. J. Trout, J. J. Schmieg, W. J. Gambogi, and A. M. Weber, "Optical photopolymers: design and applications," Adv. Mater. **10,** 1219–1224 (1998).
16. J. Yeh, A. Harton, and K. Wyatt, "Reliability study of holographic optical elements made with DuPont photopolymer," Appl. Opt. **37,** 6270–6274 (1998).
17. M. L. Jones, "Design of normal-incidence waveguide-embedded phase gratings for optical interconnects in multichip modules," Ph.D. dissertation (Georgia Institute of Technology, Atlanta, Ga., 1995).
18. A. V. Mulé, R. Villalaz, T. K. Gaylord, and J. D. Meindl, "Photopolymer-based diffractive and MMI waveguide couplers," Photon. Technol. Lett. (to be published).
19. W. DuMouchel and F. O'Brien, "Integrating a robust option into a multiple regression computing environment," in *Computing Science and Statistics: Proceedings of the 21st Symposium on the Interface*, K. Berk and L. Malone, eds. (American Statistical Association, Alexandria, Va. 1989), pp. 297–301.